Two phases of zymogen granule lifetime in mouse pancreas: ghost granules linger after exocytosis of contents

Peter Thorn[1] and Ian Parker[2]

[1] *Department of Pharmacology, University of Cambridge, Tennis Court Road, Cambridge CB2 1PD, UK*
[2] *Department of Neurobiology and Behavior, University of California Irvine, CA 92697-4550, USA*

Different cell types show widely divergent mechanisms and kinetics of exocytosis. We investigated these processes in pancreatic acinar cells by using video-rate 2-photon microscopy to image entry of extracellular dye into individual zymogen granules undergoing exocytosis. Fluorescence signals display two distinct phases; an initial peak that then decays over several seconds to a prolonged plateau. Several observations suggest that the first component reflects the binding of dye to the granule contents and their subsequent release into the acinar duct. These observations include: the peak/plateau fluorescence ratio differs between different dyes; the initial fluorescence decay mirrors the loss of granule contents as monitored by differential interference contrast microscopy; and the fall in vesicular fluorescence is accompanied by a rise in fluorescence in the adjacent duct lumen. We thus propose the use of extracellular fluorescent probes as a convenient means to monitor the kinetics of loss of proteinaceous content from secretory granules. In pancreatic acinar cells the fusion pore remains open much longer than required to ensure secretion of the granule contents, and instead the persistent empty 'ghost-granule' may act as a conduit to which secondary granules can fuse and release their contents by compound exocytosis.

(Resubmitted 11 October 2004; accepted after revision 23 December 2004; first published online 6 January 2005)
Corresponding author P. Thorn: Department of Pharmacology, University of Cambridge, Tennis Court Road, Cambridge CB2 1PD, UK. Email: pt207@cam.ac.uk

Recent improvements in imaging techniques now allow us to observe the behaviour of individual secretory vesicles in real time, revealing a wide diversity in the mechanisms and dynamics of exocytosis and endocytosis among different cell types (Jahn & Sudhof, 1999; Kasai, 1999; Holroyd *et al.* 2002; Graham *et al.* 2002; Taraska *et al.* 2003). For example, rates of exocytotic loss of vesicle contents vary widely between milliseconds (Sabatini & Regehr, 1996) to tens of seconds (Barg *et al.* 2002; Taraska *et al.* 2003). Moreover, there are striking differences in the lifetimes of vesicles after fusion, and in the mechanisms by which they are recycled. In some cells, fusion results in the rapid collapse of the vesicle and incorporation of the vesicular membrane into the plasma membrane, from where it is subsequently retrieved by endocytotic processes (Heuser & Reese, 1973; Valtorta *et al.* 2001). In striking contrast in other cell types, the fused vesicle remains intact and is recaptured during endocytosis so that it can be refilled and recycled in another round of exocytosis (Ceccarelli *et al.* 1972; Holroyd *et al.* 2002; Taraska *et al.* 2003).

Here, we have studied the specialized adaptations of exocytosis in exocrine mouse pancreatic acinar cells that secrete digestive enzymes in response to neuronal and hormonal stimuli. These enzymes are contained within secretory vesicles (zymogen granules) and exocytosis occurs exclusively on the apical plasma membrane adjacent to the acinar duct (Palade, 1975), leading to enzyme release into the gut. An unusual characteristic of pancreatic acinar cells, shared with some other cell types, is a process of compound exocytosis, whereby secretory granules deep within the cell release their contents by fusing with more superficial granules that have already fused to the plasma membrane. Compound exocytosis was first characterized by electron microscopy (Ichikawa, 1965; Amsterdam *et al.* 1969; Palade, 1975), and the sequential fusion of chains of vesicles has recently been visualized by real time optical imaging (Nemoto *et al.* 2001; Hafez *et al.* 2003; Thorn *et al.* 2004). A striking feature is that vesicles persist for minutes after fusion, and remain in continuity with the extracellular fluid through an open fusion pore (Thorn *et al.* 2004). We sought to determine whether such long

 DOI: 10.1113/jphysiol.2004.077230

post-fusion lifetimes are required to ensure emptying of the vesicle contents, or whether the persistence of empty 'ghost' vesicles may be an adaptation to support compound exocytosis.

To address these questions, we employed extracellular fluorescent dyes to monitor exocytosis by using high-speed two-photon microscopy to image entry of dye into fused vesicles (Nguyen *et al.* 2001; Thorn *et al.* 2004). Our results show a characteristic biphasic time course of the fluorescent signal as the dye enters the granules through the open fusion pore. The fluorescence signal rises rapidly to an initial peak and then decays over several seconds to a plateau that often persists for minutes. Employing a variety of approaches we conclude that the initial fluorescence peak is due to dye binding to granule contents, and that its decay reflects the secretion of these contents (together with bound dye) into the duct. The remaining fluorescence signal during the plateau phase then represents the post-exocytotic structure ('ghost') of an aqueous dye-filled granule.

Methods

Cell preparation

Male outbred mice (~25 g) were humanely killed and the pancreas removed following the local procedures and regulations of the University of California, and, for experiments conducted in the UK by the United Kingdom Home Office. Intact lobules and fragments of mouse pancreas were then prepared using a modified collagenase (CLSPA, Worthington, NJ, USA) digestion technique (Thorn *et al.* 1993). The original method was adapted to reduce the duration of collagenase treatment (to ~8 min) and to minimize the extent of mechanical trituration (~30 passes of the tissue through a 1 ml pipette). The resulting preparation was composed mainly of pancreatic lobules (thousands of cells) and fragments (~50–100 cells), which we plated onto coated (poly L-lysine; Sigma-Aldrich, USA) glass coverslips. Lobules and fragments were prepared and maintained in a NaCl-rich extracellular medium containing (mM): NaCl 140, KCl 5, $MgCl_2$ 2, $CaCl_2$ 1, glucose 10 and Hepes 10; pH adjusted to 7.4 with NaOH.

Two-photon imaging

We used a custom-made, video-rate, two-photon microscope with a 40 × oil immersion objective (NA, 1.35; Olympus) (Nguyen *et al.* 2001; Miller *et al.* 2002; Thorn *et al.* 2004) providing a resolution (full width at half maximum) of 0.26 μm lateral and 1.3 μm axial. Images were acquired at video rate (30 frames s^{-1}) and then averaged (typically 12–45 frames, except for the experiments of Fig. 5, which were acquired and analysed at video rate), stored and analysed with the MetaMorph program (Ver. 6.0, Universal Imaging, PA, USA).

To image exocytotic events we used the following water-soluble, membrane-impermeant fluorescent dyes at final concentrations in the extracellular media as indicated (all from Molecular Probes, Eugene, OR, USA): sulforhodamine B (SRB, 500 μM); Oregon Green (OG, 100 μM); and Alexa-488 (10 μM). All were visualized by femtosecond excitation at 780 nm, with emitted fluorescence collected at wavelengths of 550–650 nm (SRB), 510–555 nm (OG) and 510–555 nm (Alexa-488). In experiments where OG and SRB signals were recorded simultaneously (Fig. 2*C* and *D*) we used narrow band-pass filters (515–555 nm and 620–650 nm, respectively), which effectively eliminated bleed-through of OG fluorescence into the red channel, and reduced bleed-through of SRB fluorescence into the green channel to $< 5\%$.

We stimulated the cells either by direct application of agonist to the bathing solution or by photolysis of caged carbachol. For the latter, caged carbachol was added to the bathing solution (final concentration, 2.5–20 μM) and carbachol was liberated by illuminating a spot (~50 μm diameter) centred on the cells of interest with a high intensity UV light, as previously described (Thorn *et al.* 2004).

Imaging of fixed cells in the experiments shown in Fig. 3 was performed as above. Dye accumulation was assessed by comparing a 7.75 μm × 7.75 μm region in the apical domain with a region of the same area outside the cells.

Data are expressed as means ± S.E.M.; statistical significance was calculated using unpaired Student's *t* tests.

Protein binding to dyes

Experiments carried out to determine the behaviour of dyes in the presence of protein were done using the two-photon microscope to measure fluorescence from the centre of 100 μl droplets of dye solution prepared either in extracellular medium alone, or in medium including 10% bovine serum albumin (BSA, Sigma-Aldrich, MO, USA). To determine the amount of dye that bound to protein we loaded dye/protein solution on a 10-kDa filter (Centricon, Millipore, MA, USA) and separated the free dye by centrifugation according to the manufacturer's protocol. The fluorescence intensity of the recovered free dye solution was then compared to the intensity of the dye in protein-containing medium.

Results

Imaging single-granule exocytotic events

We imaged lobules and smaller fragments of mouse pancreatic tissue that retained the typical morphology of the distal portion of intact exocrine glands (Fig. 1*A*), where a network of branching ducts terminate at acini comprised of clusters of acinar cells enclosing an aqueous

acinar lumen. Inclusion of a fluorescent probe (SRB, OG or Alexa-488) in the extracellular bathing medium labelled the acinar lumen and the extracellular space between cells, but all these dyes were excluded from the cell interior (Fig. 1*A* right). Visualization by two-photon microscopy provided a thin optical 'slice' within the tissue, and minimized out-of-focus fluorescence from the large volume of dye in the surrounding solution. In order to more clearly visualize the behaviour of individual granules, we studied spontaneous events (which arise at a frequency of ~0.05 events cell^{-1} min^{-1} within a given optical slice), as well as responses to lower concentrations (~50 nM) of acetylcholine that evoked only sparse events in each cell. Single events appeared abruptly as fluorescent spots (diameter, ~0.7 μm; Fig. 1*E*) in the apical pole; this is consistent with dye entering single zymogen granules through the open fusion pore (Fig. 1*B*, see also event.avi in Supplementary Material). Measurements of fluorescence recorded from regions of interest centred on these spots displayed a characteristic time course composed of a rapid rise to an initial peak, followed by a decay over several seconds to a sustained plateau level (Fig. 1*C*). All three of the dyes we used gave *qualitatively* similar fluorescence signals following granule fusion (i.e. peak followed by plateau).

We first considered whether these phases may arise from changes in geometry of the granule. For example, if the granule contracted shortly after opening of the fusion pore, that would reduce the volume of aqueous dye contained within the granule causing the fluorescence to decline to a lower plateau level. To test this we plotted the average fluorescence along a line drawn through the granule centre

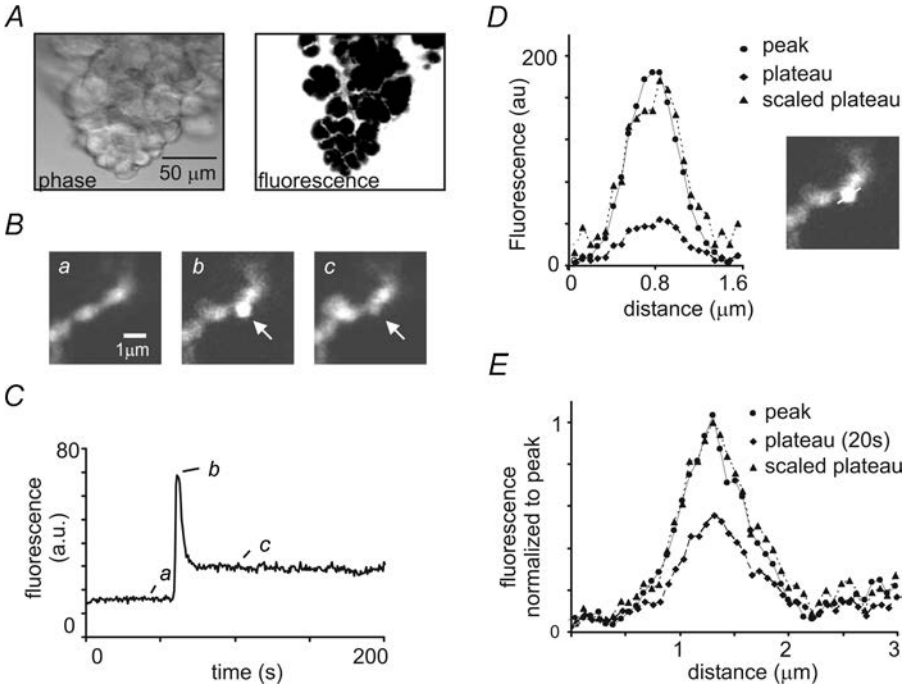

Figure 1. Morphology of pancreatic acini and imaging of individual fusion events
A, left image shows a transmitted light image of a typical pancreatic fragment used for experiments. Right image shows an optical section through the same fragment imaged using two-photon microscopy to excite a fluorescent dye (OG) in the extracellular medium. Individual cells exclude dye and appear negatively stained, whereas exocrine ducts between cells are clearly visible. *B*, an example of a single exocytotic event (indicated by arrow). The sequence of two-photon images show the initial fluorescence in an acinar lumen which traverses the image in a left bottom to right top diagonal (*a*); the abrupt appearance of a bright fluorescence spot immediately following granule fusion (*b*); and the dimmer fluorescence persisting in the granule about 30 s later (*c*). Note that further events occur in the left side of the acinar lumen. *C*, graph shows corresponding measurements of fluorescence obtained over time from a region of interest (1 μm × 1 μm) located over the granule. An initial large peak in fluorescence decays rapidly to a sustained plateau level. Times at which the images in (*B*) were captured are indicated. *D*, the fluorescence intensity of a line drawn through the granule in (*B*) at the peak (●) and at the plateau (♦) shows that although the fluorescence signal decreases, the width of the granule remains similar (scaled plateau, ▲). *E*, mean fluorescence intensity measured (with SRB as the extracellular dye) along a line drawn diametrically through individual granules. The mean fluorescence at the peak of the event (●), and at the plateau (20 s after the peak, ♦) are shown, together with the plateau fluorescence scaled to match the peak (▲). The mean width of the granules (full width at half maximal intensity) was 0.77 ± 0.05 μm ($n = 8$) at the peak and 0.77 ± 0.13 μm at the plateau (no significant difference; $P = 0.31$)

at the peak and plateau (measured 20 s after peak) of events recorded with SRB (single event Fig. 1*D* and the mean of eight events Fig. 1*E*). No detectable change in granule width was apparent. However, we cannot rule out changes in granule size below our limit of resolution, and any such changes would be amplified in the fluorescence intensity signal because vesicle volume scales as the third power of its diameter.

Different dyes give different peak/plateau ratios

We next quantified the fluorescence signals for the different dyes (Fig. 2*A*). With SRB the amplitude of the plateau (measured 10 s after the peak) was $16.1 \pm 4.9\%$ of that of the initial peak (five events), whereas the corresponding value was $34.2 \pm 5.0\%$ (13 events) for OG, and $61.97 \pm 5.3\%$ (10 events) for Alexa-488. Unpaired Student's *t* tests showed that the plateau level for Alexa-488 was significantly different from that for SRB ($P < 0.01$) and OG ($P < 0.01$), the SRB and OG plateau levels were also significantly different ($P < 0.05$).

As any change in granule volume would be expected to give similar peak–plateau relationships for the different dyes these data provide evidence that the dyes cannot be acting simply as fluorescence reporters of the water-filled volume of the granule. Instead, other dye-specific factors appear to influence their fluorescence.

One possibility is that pH-dependent changes in dye fluorescence (Lattanzio, 1990; Takahashi *et al.* 1999) might account for these observations, because the granule contents are initially acidic but neutralize following fusion as the granule interior equilibrates with the extracellular medium (De Lisle & Williams, 1987). However, even though OG fluorescence is strongly pH sensitive, it is quenched at acid pH and would thus be expected to show a rise – not fall – in fluorescence if the decay of the first component were to reflect neutralization of the vesicular pH. Moreover, we found that the fluorescence of neither SRB nor Alexa-488 is pH sensitive between pH 3.0 and 7.4 (data not shown).

Dye interaction with granule contents

We next considered whether the proteinaceous granule contents (zymogens) might interact with the dyes to increase their apparent fluorescence. The initial fluorescence peak might then result as freely diffusible dye molecules rapidly enter the granule and bind to its contents, whereas the subsequent decay of fluorescence reflects the slower loss of content and its associated dye. In that case, the fluorescence during the plateau phase would reflect simply the amount of aqueous dye remaining in the granule.

To facilitate further analysis we thus normalized records obtained with different dyes to the same plateau

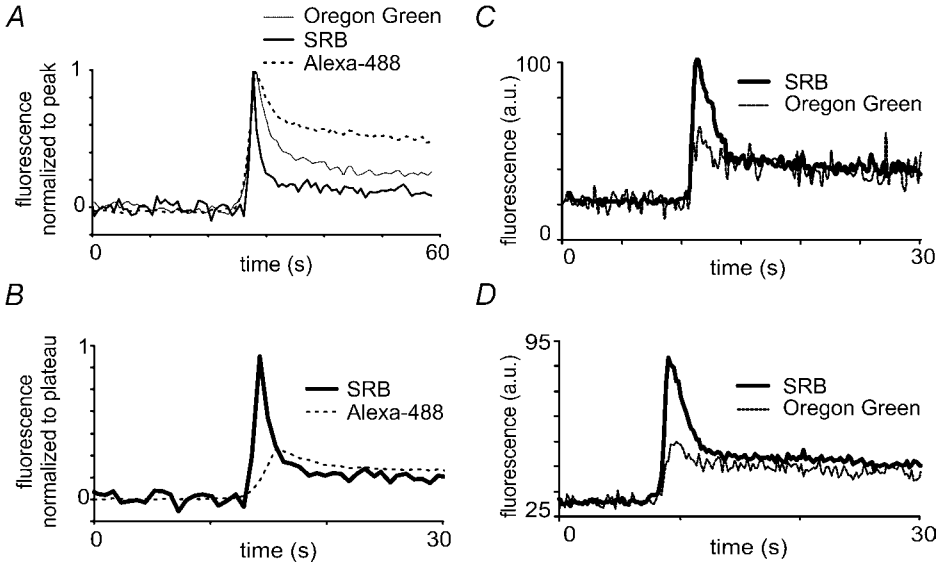

Figure 2. Different fluorescent dyes show qualitatively similar kinetic signals following fusion events but display large differences in relative amplitudes of the peak and plateau components
A, traces were derived from images like those shown in Fig. 1*B*, and represent mean kinetics of several events imaged with three different dyes (OG, $n = 13$; SRB, $n = 5$; Alexa-488, $n = 10$), after normalizing to the initial peak fluorescence. All records show spontaneous events in unstimulated cells. *B*, comparison of the decay phase of the initial fluorescence transient, after normalizing to the plateau level. Traces show mean fluorescence recorded in separate experiments with SRB (thick line, $n = 5$) and Alexa-488 (dashed line, $n = 9$). *C*, simultaneous traces of SRB and OG fluorescence during an individual granule event, obtained using dual-channel imaging with extracellular solution including both dyes. *D*, mean records from nine events (all spontaneous) obtained using simultaneous, dual-channel imaging of SRB and OG fluorescence.

level. Figure 2*B* compares mean fluorescence signals obtained using SRB ($n = 5$ granules) and Alexa-488 ($n = 9$), after normalizing to the plateau fluorescence, and demonstrates the dramatically greater initial peak seen with SRB. Moreover, simultaneous records of SRB and OG signals, obtained using a mixture of both dyes in the bathing solution and dual photomultiplier detectors at appropriate wavelengths (Fig. 2*C* and *D*), showed consistent differences in peak/plateau ratios. The plateau level of fluorescence measured 10 s after the peak was $31.7 \pm 3.8\%$ ($n = 8$) of the peak amplitude for SRB, as compared to $55.9 \pm 5.7\%$ for OG (significant using a Student's *t* test, $P < 0.01$). Thus the differences in peak/plateau ratios obtained with the dyes alone are still seen when dyes are imaged simultaneously.

The absolute values of the peak/plateau ratios were different when the dyes were imaged separately (as in Fig. 2*A*), as compared to when they were imaged simultaneously. It is not clear whether this is due to differences in the optical setup needed for simultaneous measurements, or whether it may reflect competition between dyes for binding sites. The important point is that peak/plateau ratios differ appreciably between various dyes, and that differences persist even when two dyes are imaged simultaneously. Thus, the kinetic changes in dye fluorescence cannot simply reflect volume changes of the granule, but instead the fluorescence properties of different dyes appear to be differentially affected by the contents of the granule.

Characteristics of dye binding to proteins

To characterize how the dye behaviours are modified in the presence of proteins, we measured their fluorescence when equilibrated with a 10% solution of BSA. With respect to their fluorescence in aqueous solution, SRB showed only a slight decrease on addition of BSA, whereas both Oregon Green and Alexa-488 were quenched to $< 25\%$ (Table 1). To then determine the amount of dye bound to protein we filtered the BSA–dye solutions through a 10-kDa cut-off filter (BSA has a molecular weight of ~70 kDa), and measured the fluorescence of the filtrate. All three dyes bound strongly to BSA (Table 1).

Although these data do not replicate the environment of the granule, and give no information regarding the kinetics of the dyes on the time scale of granule fusion and filling, they do show that whereas all three dyes bind strongly to proteins, they are differentially quenched. The fluorescence signal measured from vesicles is thus expected to depend on the combined effects of accumulation and quenching as dyes bind to the granule contents. Specifically, SRB bound strongly to protein, but showed little quenching, consistent with the notion that accumulation of dye by binding to granule contents may explain the large initial fluorescence transient seen with this dye. In contrast, OG and Alexa-488 binding were accompanied by a strong quenching, so that these dyes would be expected to show smaller initial fluorescence transients.

Table 1. Measurements of in vitro binding of fluorescent dyes to protein (BSA) and consequent quenching of fluorescence

	Fluorescence in presence of protein (% control)	Percentage of dye bound to protein
SRB	88	65
Oregon Green	25	87
Alexa-488	20	83

See text for details.

To further test this hypothesis, and determine dye behaviour with the actual granule contents, we imaged paraformaldehyde-fixed, Triton X-100 (0.1%)-treated acinar cells that were bathed in SRB (0.5 mM) or OG (100 μM). After a short period of equilibration, cells were imaged with the two-photon microscope (Fig. 3). In both cases the dyes accumulated in the cells raising their fluorescence above that of the surrounding media. Regions of interest (7.75 μm × 7.75 μm) in the granular apical pole region were 3.66 ± 0.93 ($n = 5$) times brighter than the bathing solution surrounding the cell for SRB, and 1.18 ± 0.03 ($n = 4$) times brighter for OG ($P < 0.05$). These data are consistent with differences in the peak/plateau fluorescence ratios observed following granule fusion in live cells shown in Fig. 2.

We conclude therefore that the initial large peak of SRB fluorescence following granule fusion arises because dye entering the granule binds to protein contents, resulting in an effective concentration increase. The subsequent decay in fluorescence then reflects the loss of protein content together with its associated bound dye, with the final plateau level corresponding to the dye remaining in free aqueous solution in the 'empty' granule.

Loss of granule contents measured by differential interference contrast microscopy

A key point in the above interpretation is that the decay of the initial transient of SRB fluorescence reflects the loss of zymogen contents from the granule into the secretory duct. To verify whether this is the case, we independently measured changes in granule contents by means of differential interference contrast (DIC) microscopy (Ishihara *et al.* 2000). We observed increases in light intensity at discrete spots in the apical pole following stimulation by acetylcholine (Fig. 4*A*). The mean rise time of the DIC signal matched well to the falling phase of SRB fluorescence signals measured separately in other experiments (Fig. 4*B*). Single exponential fits to the decay of the SRB fluorescence and rise of the DIC signal gave respective time constants of 5.6 ± 0.8 s ($n = 13$), and

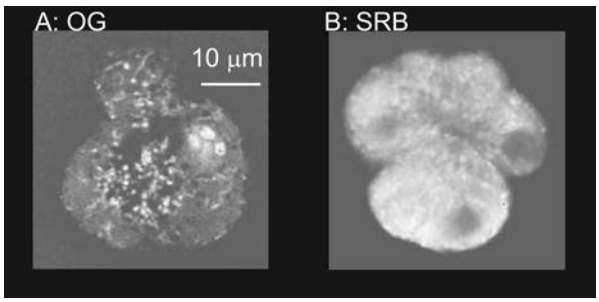

Figure 3. Two-photon imaging of fixed and permeabilized pancreatic acinar cells shows differential dye accumulation in secretory granules
Fixed cells were permeabilized with Triton X-100 and imaged with a two-photon microscope in the presence of either OG (*A*) or SRB (*B*) in the bathing solution. The images were normalized with respect to the brightness of extracellular fluorescence. Both dyes stained the cells, indicating binding to cell proteins, but fluorescence in the cell compared to fluorescence in the surrounding media showed that dye accumulation for SRB was much larger than for OG.

4.37 ± 0.6 s ($n = 7$), in agreement with the idea that both signals reflect the time course of loss of granule contents.

Are granules empty during the plateau phase of the fluorescence signal?

Following the initial fluorescence transient, plateau levels of fluorescence persist for as long as 12 min (Thorn *et al.* 2004), indicating that the granule is in stable equilibrium with the external medium and may have lost most, if not all of its protein contents. To test this, we used data from the experiments of Fig. 2*C* and *D* to measure the ratio of SRB fluorescence to OG fluorescence in vesicles at the peak and at the plateau, and compared this to the fluorescence ratio in the bathing solution (measured in region outside the acini of $\sim$10 μm $\times$ 10 μm). We reasoned that at the peak, dye binding to granule contents would result in a higher SRB/OG fluorescence ratio than in the aqueous external medium. However during the plateau, the ratio inside the granule should be similar to that outside if the granule were devoid of proteinaceous contents. Measurements showed a peak SRB/OG fluorescence ratio of 2.4 ± 0.35 times larger than that outside ($n = 9$), whereas during the plateau the ratio was only 1.2 ± 0.37 times greater ($n = 8$). Thus, the fluorescence during the plateau phase of the fluorescence signal is consistent with that expected if the granule contains only an aqueous solution of dye after releasing almost all of its contents by exocytosis.

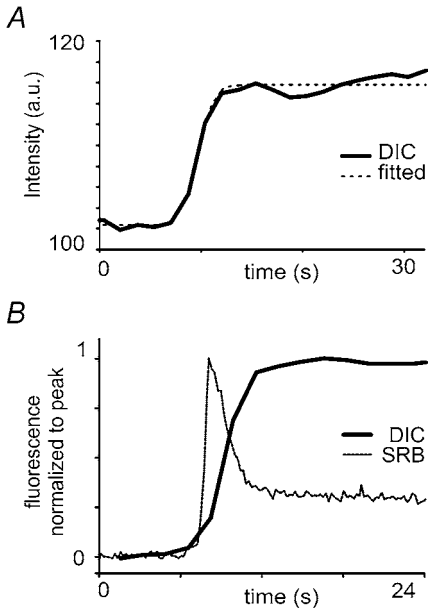

Figure 4. Optical signals measured by DIC microscopy during granule emptying
A, thick trace shows transmitted light intensity measured by DIC microscopy from a region of interest (0.5 μm $\times$ 0.5 μm) centred on a granule undergoing exocytosis in response to stimulation with caged carbachol. Dashed line is a single exponential fit to the rising phase. *B*, thick trace shows the mean DIC signal during seven secretory events, and the thin trace shows the mean SRB signal (reproduced from Fig. 2*D*) derived in other experiments. Both traces are scaled to the same peak magnitude, and are aligned in time to their onset.

Fusion events are followed by a fluorescence increase in the adjacent lumen

If the initial fluorescence peak represents dye binding to vesicular contents, the subsequent loss of contents might be associated with a transient increase in fluorescence in the adjacent lumen as the protein (and the dye bound to it) passes out of the granule. This was indeed the case. Measurements of SRB fluorescence from a region of interest located in the acinar lumen closely adjacent to fusing granules showed a small rise throughout the period when the granule fluorescence was falling (Fig. 5, see also event2.avi in Supplementary Material). Quantitative measurements were made by placing regions of interest (0.625 μm $\times$ 0.625 μm) over the acinar lumen adjacent to granules undergoing exocytosis (Fig. 5*Ac*). To compare records across experiments the lumen fluorescence was normalized to the peak fluorescence changes. This mean normalized fluorescence increased to $45.09 \pm 15.3\%$ ($n = 14$) when measured 6 s after the peak of the adjacent granule event ($P < 0.05$ when compared to the normalized fluorescence 3 s before granule fusion) (Fig. 5*B*, ●). Thus the temporal correlation between the rise in luminal fluorescence and fall in granule fluorescence is consistent with exocytotic movement of granule contents and associated bound dye.

Discussion

Our data provide new insights into the mechanisms of secretion in pancreatic acinar cells. Previous reports have indicated that zymogen granules (secretory vesicles) persist for a long time after fusion with the apical cell membrane (Nemoto *et al.* 2001; Thorn *et al.* 2004). We now show that this lifetime can be divided into two phases.

The first involves the loss of granule contents over several seconds following opening of the fusion pore. Subsequent endocytosis is delayed, and the granule persists for a long time (tens of seconds or minutes) with its fusion pore open during its second phase as a substantially empty 'ghost' (Thorn *et al.* 2004). The long lifespan of the ghost granules is therefore not needed to ensure secretion of their contents, but instead is likely to be an adaptation to permit compound exocytosis by subsequent fusion of secondary granules to the ghost.

Fluorescent dyes report granule content

Our finding of rapid exocytosis of zymogen granule contents is based on fluorescence measurements of extracellular dye entry into granules following their fusion.

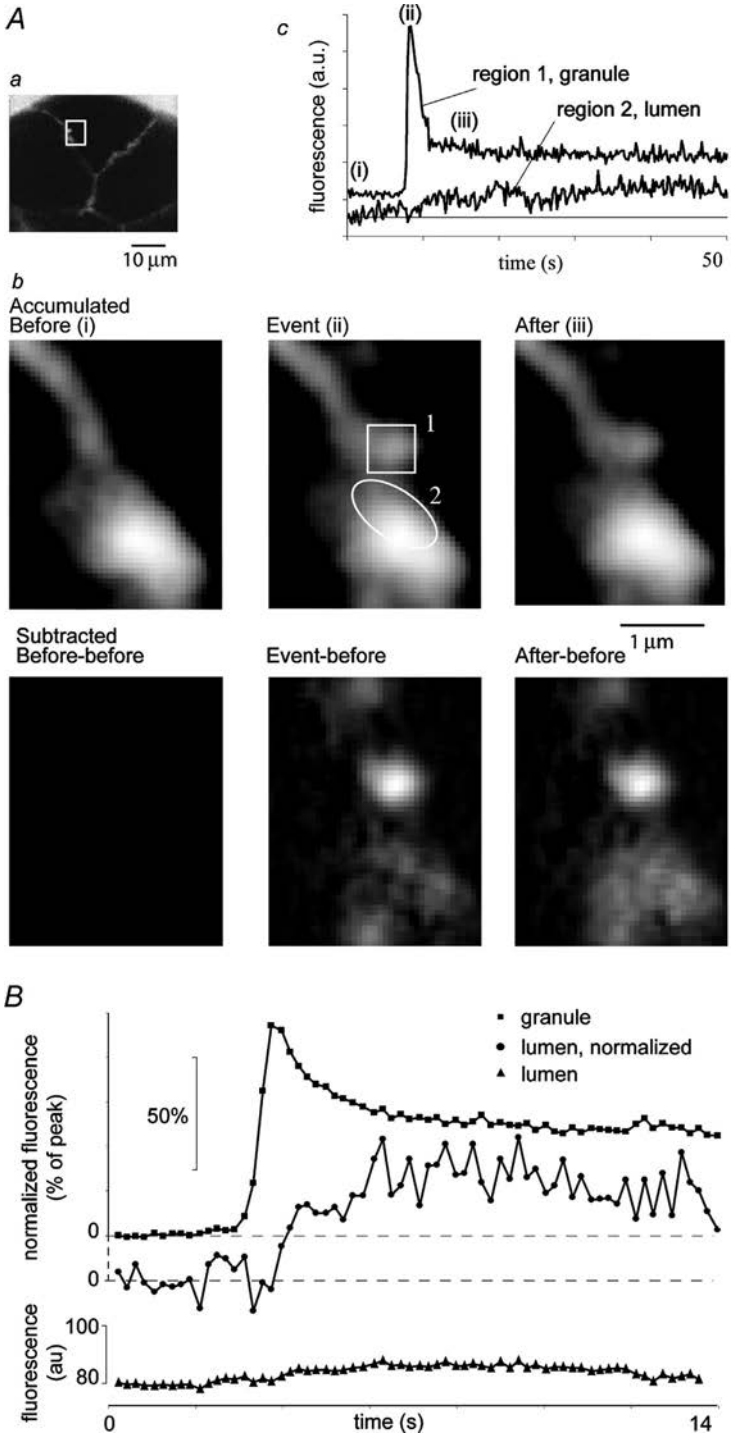

Figure 5. Fluorescence decrease in granules is accompanied by a transient increase in fluorescence in the adjoining acinar lumen
A, representative example of a single vesicle fusion event followed by a slow rise in luminal fluorescence. *a*, low magnification image showing three acinar cells. SRB was present in the extracellular solution. *b*, enlarged views of the acinar lumen region marked by the box in *a*. Each panel is an average of 37 consecutive frames (captured every 200 ms). The upper row of images show (left to right) basal fluorescence in the acinar lumen, an exocytotic event, and elevated fluorescence in the adjacent acinar lumen following the event. Regions of interest marked on the middle image were used to measure the traces shown in (*c*). The lower row of images were obtained after subtracting the initial basal fluorescence. *c*, traces show fluorescence changes measured from regions of interest as indicated in *b*. *B,* graph shows changes in SRB fluorescence measured from the vesicle and adjacent acinar lumen averaged from 16 recordings as in *A*. Traces show (from top to bottom): granule fluorescence, normalized to peak; luminal fluorescence, normalized to its peak; and the raw mean luminal fluorescence trace.

Fluorescence signals show biphasic kinetics; a rapid (< 1 s) rise to a peak, followed by a decay over several seconds to a low plateau that persists for many seconds or minutes. Based on several lines of evidence we conclude that the biphasic fluorescence kinetics arise from the binding of dye to granule contents which are subsequently lost into the duct lumen. (1) We did not observe any measurable change in granule width associated with the decay of the initial fluorescence transient, suggesting that the decay does not result from a decrease in granule volume. (2) Different dyes showed different peak–plateau relationships, indicating that the biphasic fluorescence profile is determined, at least in part, by the specific properties of different dyes in the intra-granule environment. (3) In agreement with this, the dyes we employed showed differential binding and fluorescence quenching in the presence of proteins (BSA). (4) Dye accumulation in the granule-dense apical domain of fixed, permeabilized pancreatic acinar cells matched that expected from the live-cell imaging experiments. (5) The time course of the fluorescence decay from peak to plateau closely mirrored that of differential interference contrast signals that are presumed to reflect loss of granule contents. (6) The SRB/OG fluorescence ratio in the granule during the plateau is similar to that of the bathing medium, as expected if the ghost granule contains only an aqueous solution of dye. (7) The decay of granule fluorescence was accompanied by a transient rise in fluorescence in the adjoining duct. This is consistent with the exit of dye bound to granule contents, although we cannot rule out other possibilities such as possible postexocytotic changes in dye–protein binding characteristics.

Taken together these data support the idea that extracellular dye enters a granule upon the opening of the fusion pore and rapidly accumulates on the intra-granule contents. The subsequent decay in fluorescence then occurs due to the loss of granule contents and the concomitant loss of bound dye. Fluorescence remaining during the plateau phase most likely represents dye present in free aqueous solution in an empty ghost vesicle, although we cannot exclude the possibility that a small fraction of the vesicle contents may persist during this phase. Measurements of vesicular fluorescence thus offer a promising means to monitor the loss of proteinaceous granule contents.

Methods for measuring loss of vesicle contents upon exocytosis

A number of different methods have been used to follow exocytotic loss of vesicle content. These are variously applicable to measuring secretion, and are discussed below along with our new method.

One method involves the tagging of a known vesicle protein with a fluorescent protein, so as to image its loss during exocytosis (Barg *et al.* 2002; Taraska *et al.* 2003; Ohara-Imaizumi *et al.* 2002; Tsuboi *et al.* 2000). A key advantage is that the decrease in fluorescence provides a direct measure of loss of the fluorescent protein. Disadvantages include the difficulty of expressing exogenous proteins in acutely isolated cell preparations, the possibility that over-expressed proteins may not follow the behaviour of native proteins and the susceptibility of fluorescent proteins to pH and other environmental factors.

An alternative approach utilizes DIC microscopy of vesicles as an indirect measure of loss of vesicle contents (Ishihara *et al.* 2002). This provides an indication of the time course of loss of vesicle content, but is difficult to quantify, and signals may be contaminated by factors (e.g. pH change) other than the content loss.

A final method, of which our approach is a novel variant, tracks the loss of vesicle contents through the use of vital dyes. This was first demonstrated by Angleson *et al.* (1999) who found that that the lipophilic probe FM1-43 also stained the contents of lactotroph granules, which could then be imaged in real time to follow granule content loss. However, FM1-43 binding to granule contents has not generally been observed, and in our hands FM1-43 does not stain zymogen granule contents in pancreatic acinar cells (Thorn *et al.* 2004; see also Giovannucci *et al.* 1998 but see Gaisano *et al.* 2001). Instead, the approach we describe is based on aqueous protein-binding dyes that do not have the complication of binding to lipids. This method is especially amenable to pancreatic acinar cells, where the granules are densely packed with protein and the duct is likely to contain little protein at rest. It remains to be determined whether it will be more generally applicable to other cell types that secrete proteins. For example, Takahashi *et al.* (2002) present evidence that fluorescence signals from granules in pancreatic β cells are consistent simply with dye occupying the aqueous volume of the granule, and not with dye binding to content.

Time course of granule content loss

By measuring the decay of the initial fluorescence transient, we estimate that fused zymogen granules lose their contents (primarily peptide enzymes, e.g. amylase; MW, $\sim$50 kDa) with a time constant of about 6 s. This rate is similar to measurements obtained using green fluorescent protein (GFP)-tagged peptides to monitor secretion in other cell types. For example, loss of enhanced, EGFP-islet amyloid polypeptide in an insulin-secreting cell line occurs over 1–10 s (Barg *et al.* 2002), and loss of enhanced, EGFP-neuropeptide Y from vesicles in PC-12 cells is complete within 10 s (Taraska *et al.* 2003). In contrast to these measures of peptide release, indirect measures of vesicular release of non-peptide neurotransmitters at synapses are some

50 000 times faster (Sabatini & Regehr, 1996), pointing to an enormous diversity in kinetics of exocytosis among diverse cell types that probably reflects both functional and structural differences (Kasai, 1999). In contrast to neuronal signalling, there is no special need for rapid secretion of digestive enzymes; indeed, transport along the duct is probably much slower than emptying from the granule. Moreover, mechanistic constraints will limit the speed of release from zymogen granules. In contrast to the almost instantaneous release of small-molecule neurotransmitters following kiss-and-collapse fusion, the larger granules in pancreatic acini remain intact and their protein contents must escape through the restricted dimensions of the intact fusion pore.

Structural stablization of ghost granules

Zymogen granules show little or no decrease in volume after exocytosis (Fig. 1). Because the granule lipid membrane itself has no structural integrity, some other mechanism must structurally stabilize the granule. One candidate is the actin cytoskeleton, which forms a coat around individual granules (Valentijn *et al.* 2000; Nemoto *et al.* 2004). New evidence indicates that this F-actin coat is formed after opening of the fusion pore and may therefore be involved in maintaining the structure of the primary vesicle to prevent its collapse and, possibly, to facilitate secondary fusion events (Turvey & Thorn, 2004).

Conclusions

In conclusion our data suggest that, after fusion with the plasma membrane, loss of content occurs relatively rapidly. The subsequent persistence of the empty granule provides a target for the fusion of secondary granules and a conduit for the loss of their contents.

References

Amsterdam A, Ohad I & Schramm M (1969). Dynamic changes in the ultrastructure of the acinar cell of the rat parotid gland during the secretory cycle. *J Cell Biol* **41**, 753–773.

Angleson JK, Cochilla AJ, Kilic G, Nussinovitch I & Betz WJ (1999). Regulation of dense core release from neuroendocrine cells revealed by imaging single exocytic events. *Nat Neurosci* **2**, 440–446.

Barg S, Olofsson CS, Schriever-Abeln J, Wendt A, Gebre-Medhin S, Renstrom E & Rorsman P (2002). Delay between fusion pore opening and peptide release from large dense-core vesicles in neuroendocrine cells. *Neuron* **17**, 287–299.

Ceccarelli B, Hurlbut WP & Mauro A (1972). Depletion of vesicles from frog neuromuscular junctions by prolonged tetanic stimulation. *J Cell Biol* **54**, 30–38.

De Lisle RC & Williams JA (1987). Zymogen granule acidity is not required for stimulated pancreatic protein secretion. *Am J Physiol* **253**, G711–G719.

Gaisano HY, Lutz MP, Leser J, Sheu L, Lynch G, Tang L, Tamori Y, Trimble WS & Salapatek AM (2001). Supramaximal cholecystokinin displaces Munc18c from the pancreatic acinar basal surface, redirecting apical exocytosis to the basal membrane. *J Clin Invest* **108**, 1597–1611.

Giovannucci DR, Yule DI & Stuenkel EL (1998). Optical measurement of stimulus-evoked membrane dynamics in single pancreatic acinar cells. *Am J Physiol* **275**, C732–C739.

Graham ME, O'Callaghan DW, McMahon HT & Burgoyne RD (2002). Dynamin-dependent and dynamin-independent processes contribute to the regulation of single granule release kinetics and quantal size. *Proc Natl Acad Sci U S A* **99**, 7124–7129.

Hafez I, Stolpe A & Lindau M (2003). Compound exocytosis and cumulative fusion in eosinophils. *J Biol Chem* **278**, 44921–44928.

Heuser JE & Reese TS (1973). Evidence for recycling of synaptic vesicle membrane during transmitter release at the frog neuromuscular junction. *J Cell Biol* **57**, 315–344.

Holroyd P, Lang T, Wenzel D, De Camilli P & Jahn R (2002). Imaging direct, dynamin-dependent recapture of fusing secretory granules on plasma membrane lawns from PC12 cells. *Proc Natl Acad Sci U S A* **99**, 16806–16811.

Ichikawa A (1965). Fine structural changes in response to hormonal stimulation of the perfused canine pancreas. *J Cell Biol* **24**, 369–385.

Ishihara Y, Sakurai T, Kimura T & Terakawa S (2000). Exocytosis and movement of zymogen granules observed by VEC-DIC microscopy in the pancreatic tissue en bloc. *Am J Physiol Cell Physiol* **279**, C1177–C1188.

Jahn R & Sudhof TC (1999). Membrane fusion and exocytosis. *Ann Rev Biochem* **68**, 863–911.

Kasai H (1999). Comparative biology of Ca^{2+}-dependent exocytosis: implications of kinetic diversity for secretory function. *Trends Neurosci* **22**, 88–93.

Lattanzio FA (1990). The effects of pH and temperature on fluorescent calcium indicators as determined with Chelex-100 and EDTA buffer systems. *Biochem Biophys Res Commun* **171**, 102–108.

Miller MJ, Wei SH, Parker I & Cahalan MD (2002). Two-photon imaging of lymphocyte motility and antigen response in intact lymph node. *Science* **296**, 1869–1873.

Nemoto T, Kimura R, Ito K, Tachikawa A, Miyashita Y, Iino M & Kasai H (2001). Sequential-replenishment mechanism of exocytosis in pancreatic acini. *Nat Cell Biol* **3**, 253–258.

Nemoto T, Kojima T, Oshima A, Bito H & Kasai H (2004). Stabilization of exocytosis by dynamic F-actin coating of zymogen granules in pancreatic acini. *J Biol Chem* **279**, 37544–37550.

Nguyen QT, Callamaras N, Hsieh C & Parker I (2001). Construction of a two-photon microscope for video-rate $Ca^{(2+)}$ imaging. *Cell Calcium* **30**, 383–393.

Ohara-Imaizumi M, Nakamich Y, Tanaka T, Katsuta H, Ishida H & Nagamatsu S (2002). Monitoring of exocytosis and endocytosis of insulin secretory granules in the pancreatic b-cell line MIN6 using pH-sensitive green fluorescent protein (pHluorin) and confocal laser microscopy. *Biochem J* **363**, 73–80.

Palade G (1975). Intracellular aspects of the process of protein synthesis. *Science* **189**, 347–368.

Sabatini BL & Regehr WG (1996). Timing of neurotransmission at fast synapses in the mammalian brain. *Nature* **384**, 170–172.

Takahashi A, Camacho P, Lechleiter J & Herman B (1999). Measurement of intracellular calcium. *Physiol Rev* **79**, 1089–1125.

Takahashi N, Kishimoto T, Nemoto T, Kadowaki T & Kasai H (2002). Fusion pore dynamics and insulin granule exocytosis in the pancreatic islet. *Science* **297**, 1349–1352.

Taraska JW, Perrais D, Ohara-Imaizumi M, Nagamatsu S & Almers W (2003). Secretory granules are recaptured largely intact after stimulated exocytosis in cultured endocrine cells. *Proc Natl Acad Sci U S A* **100**, 2070–2075.

Thorn P, Fogarty KE & Parker I (2004). Zymogen granule exocytosis is characterized by long fusion pore openings and preservation of vesicle lipid identity. *Proc Natl Acad Sci U S A* **101**, 6774–6779.

Thorn P, Lawrie AM, Smith PM, Gallacher DV & Petersen OH (1993). Local and global cytosolic Ca^{2+} oscillations in exocrine cells evoked by agonists and inositol trisphosphate. *Cell* **74**, 661–668.

Tsuboi T, Zhao C, Terakawa S & Rutter GA (2000). Simultaneous evanescent wave imaging of insulin vesicle membrane and cargo during a single exocytotic event. *Curr Biol* **10**, 1307–1310.

Turvey MR & Thorn P (2004). Lysine-fixable dye tracing of exocytosis shows F-actin coating is a step that follows granule fusion in pancreatic acinar cells. *Pflugers Arch* **448**, 552–555.

Valentijn JA, Valentijn K, Pastore LM & Jamieson JD (2000). Actin coating of secretory granules during regulated exocytosis correlates with the release of rab3D. *Proc Natl Acad Sci U S A* **97**, 1091–1095.

Valtorta F, Meldolesi J & Fesce R (2001). Synaptic vesicles: is kissing a matter of competence? *Trends Cell Biol* **11**, 324–328.

Acknowledgements

We thank Mike Edwardson for comments on the manuscript. This work was funded by a Wellcome Trust travel award (P.T. and I.P.), a Medical Research Council (UK) project grant (G0000214 to P.T.) and a grant from the National Institutes of Health (GM48071 to I.P.).

Supplementary Material

The online version of this paper can be accessed at:
DOI: 10.1113/jphysiol.2004.077230
http://jp.physoc.org/cgi/content/full/jphysiol.2004.077230/DC1
and contains Supplementary Material consisting of two movies. Movie 1 is a sequence of a single exocytotic event recorded using SRB. Images are 7.7 μm wide and the clip is 40 s long. Movie 2 is a sequence of the event observed in Fig. 5 is shown, recorded using SRB. During the sequence the subsequent increase in fluorescence in the duct is seen. Images are 2.56 μm wide and the clip is 62 s long.